ADVANCES IN ATMOSPHERIC SCIENCES, VOL. 25, NO. 2, 2008, 306–318

Consistency Problem with Tracer Advection in the Atmospheric Model GAMIL

ZHANG Kai*[1,3] (张 恺), WAN Hui[1,3] (万 慧), WANG Bin[1] (王 斌), and ZHANG Meigen[2] (张美根)

[1] *State Key Laboratory of Numerical Modeling for Atmospheric Sciences and Geophysical Fluid Dynamics (LASG), Institute of Atmospheric Physics, Chinese Academy of Sciences, Beijing* 100029

[2] *State Key Laboratory of Atmospheric Boundary Layer Physics and Atmospheric Chemistry (LAPC), Institute of Atmospheric Physics, Chinese Academy of Sciences, Beijing* 100029

[3] *Graduate University of the Chinese Academy of Sciences, Beijing* 100049

(Received 22 November 2006; revised 27 April 2007)

ABSTRACT

The radon transport test, which is a widely used test case for atmospheric transport models, is carried out to evaluate the tracer advection schemes in the Grid-Point Atmospheric Model of IAP-LASG (GAMIL). Two of the three available schemes in the model are found to be associated with significant biases in the polar regions and in the upper part of the atmosphere, which implies potentially large errors in the simulation of ozone-like tracers. Theoretical analyses show that inconsistency exists between the advection schemes and the discrete continuity equation in the dynamical core of GAMIL and consequently leads to spurious sources and sinks in the tracer transport equation. The impact of this type of inconsistency is demonstrated by idealized tests and identified as the cause of the aforementioned biases. Other potential effects of this inconsistency are also discussed. Results of this study provide some hints for choosing suitable advection schemes in the GAMIL model. At least for the polar-region-concentrated atmospheric components and the closely correlated chemical species, the Flux-Form Semi-Lagrangian advection scheme produces more reasonable simulations of the large-scale transport processes without significantly increasing the computational expense.

Key words: numerical climate modelling, tracer transport, advection scheme, consistency

DOI: 10.1007/s00376-008-0306-z

1. Introduction

The atmospheric general circulation model (AGCM) is an indispensable tool to understand the climate system and predict future climate change. The large-scale transport process of important atmospheric components in AGCMs is calculated by the numerical advection scheme. It immediately affects the spatial and temporal distribution of tracers such as the water vapor and hence have a comprehensive impact on the simulated hydrological cycle and all the related climate processes. For the past few years the traditional physical climate system models have been evolving towards the comprehensive earth system models which various chemical and biological processes are involved. A large number of chemical species, such as ozone and aerosols, are introduced to the model system, and pose new challanges to the numerical schemes for transport simulation.

The GAMIL model developed at the Institute of Atmospheric Physics in Beijing is a global atmospheric model with a finite-differece dynamical core (Wang et al., 2004; Wan et al., 2006). The first model version has two schemes for the water vapor advection: the Two-step Shape Preserving Advection Scheme (TSPAS) (Yu, 1994) and the Multidimensional Positive Definite Advection Transport Algorithm (MPDATA) (Smolarkiewicz and Grabowski, 1990). Both schemes are mass conservative, shape-preserving and positive definite, although TSPAS is more efficient in regard to computational expense.

MPDATA is a flexible algorithm that has been ex-

*Corresponding author: ZHANG Kai, zhangkai@mail.iap.ac.cn

tensively modified and implemented over more than twenty years in various application such as advection modeling (Smolarkiewicz and Grabowski, 1990) and nonoscillatory interpolation (Smolarkiewicz and Grell, 1992). This algorithm is based on the donor-cell advection scheme and belongs to the general class of Lax-Wendroff methods. The basic idea is to compensate the second-order error of donor-cell advection by the iterated upwind approximation.

TSPAS is also a finite-difference advection scheme. For each temporal integration step, the Lax-Wendroff scheme with an adjusted time increment is used first as a pre-estimator to get the first-guess of the tracer concentration at the next time step. A shape-preserving check is then performed at each grid point. At those locations where the shape-preserving requirement is fulfilled, the Lax-Wendroff scheme is then used for the temporal integration; elsewhere the upstream scheme is used. Combining the advantage of small dispersion error in the upstream scheme and small dissipation error in the Lax-Wendroff scheme, TSPAS has been performing quite well in the simulations of heavy rainfall and tropical cyclones in East Asia.

Recently the Flux-Form Semi-Lagrangian transport schemes (FFSL) proposed by Lin and Rood (1996) (hereafter LR96) have been implemented in GAMIL as the third option of the advection scheme. The FFSL package includes a family of finite-volume schemes that are forward-in-time, upstream-biased and oscillation-free (with the optional monotonicity constraint). The semi-Lagrangian feature of FFSL ensures computational stablity when the Courant number exceeds unity in the longitudinal direction, hence imposes less restrictive constraints over the polar regions. The flux-form discretization, on the other hand, guarantees the mass conservation. The FFSL algorithm has been employed in many AGCMs and atmospheric chemistry transport models (see, e.g., Chin et al., 2000; Rotman et al., 2001; Roeckner et al., 2003).

Prior to the present work the performance of the FFSL scheme in the GAMIL model has not been assessed. The TSPAS and MPDATA schemes have been used for water vapor transport only, with some preliminary evaluations focusing on the general circulation of the atmosphere. Currently the aerosol and atmospheric chemistry modules of GAMIL are under development. Many of the newly introduced species have their own distinct properties. For example, methane (CH_4) is an important greenhouse gas which has a much longer lifetime than the water vapor; ozone (O_3), also a greenhouse gas, is very active in chemical reactions and has higher concentrations in the upper atmosphere. It is therefore necessary to carry out comprehensive comparisons between the available advection schemes via carefully designed tests, so that useful information can be obtained for choosing appropriate advection schemes for various tracers. The result of this study should be very helpful in providing a sound basis for simulating chemical processes. In section 2 of this paper, results of the radon transport test are described, and some evident biases are detected. Section 3 addresses the source of the biases as analyzed theoretically and it is verified with an idealized numerical experiment. Additional discussions are presented in section 4, and conclusions presented in section 5.

2. Results of the radon transport test

The radon (^{222}Rn) transport test is now widely used for the evaluation and intercomparison of tracer transport models and schemes (Jacob and Prather, 1990; Genthon and Armengaud, 1995; Jacob et al., 1997; Rasch et al., 2000). The species of interest, radon, is a natural radioisotope emitted ubiquitously from soils and removed from the atmosphere by radioactive decay with an e-folding lifetime of 5.5 days. According to the World Climate Research Program (WCRP) 1995 protocol (Rasch et al., 2000), the test assumes a uniform emission of 1.0 atoms cm^{-2} s^{-1} from the land between 60°S and 60°N, and 0.5 atoms cm^{-2} s^{-1} from the land between 60°N and 70°N except Greenland. With radon treated as a passive tracer, climate simulations are carried out with the GAMIL model using climatological sea surface temperature and sea ice distribution as the lower boundary conditions. Meteorological fields at the initial step are interpolated from the ECMWF 40 Years Re-Analysis (ERA40) data (Uppala et al., 2005) for 1 January 1979. The initial concentration of radon is set to zero. Each simulation proceeds six years with the first year discarded as the spin-up period. Five-year mean radon concentration is then calculated and compared with observations and results from other models.

It should be noted that distributions of radon in AGCMs are affected not only by synoptic-scale transport, but also by subgrid processes such as cumulus convection and boundary layer mixing. Nonetheless, the former is the major factor that determines the global distribution of radon concentration and is the focus here. In order to isolate the impact of the large-scale transport from other factors, the test is conducted using all the three advection schemes in GAMIL while keeping the rest parts of the model exactly the same. By intercomparison of results from these three realizations, we are able to identify errors that are caused by specific features of each advection schemes. A comprehensive evaluation of the results from the radon transport test, including investigation

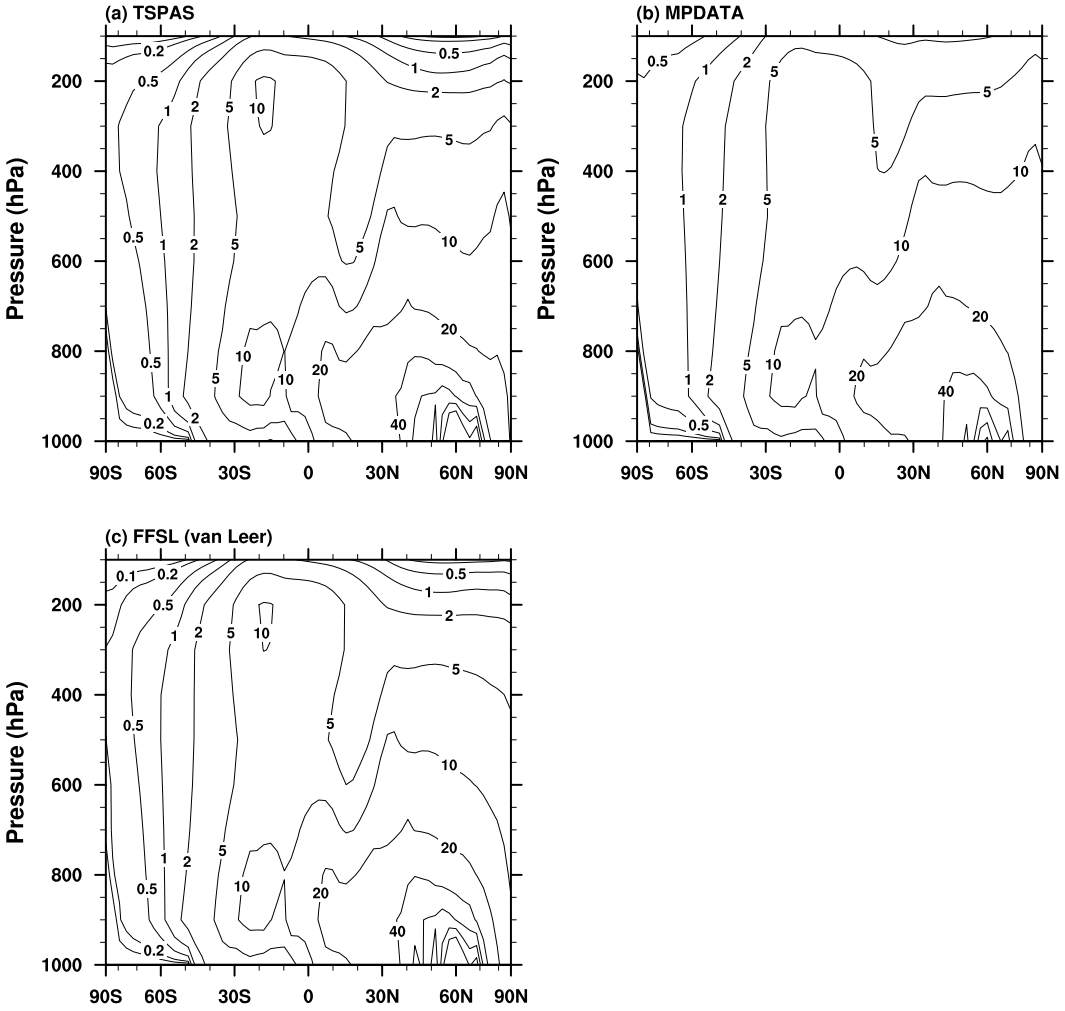

Fig. 1. Simulated zonal mean radon concentration in boreal winter by GAMIL using the (a) TSPAS, (b) MPDATA, and (c) FFSL (van Leer) advection scheme, respectively. Results shown here are the averages over December, January and February. (units: pCI m^{-3} STP)

of the roles of other processes, is presented in elsewhere.

Figure 1 shows the 5-year-mean zonally averaged radon concentration in boreal winter simulated by GAMIL using three advection schemes. Note that the FFSL advection package is actually a family of schemes. We only present here in Fig. 1c the results calculated with the piecewise linear (i.e., the van Leer type) approximation. (Experiments using other options, for example the piecewise parabolic approximation with different monotonicity constraints, have also been carried out. The results are very similar to Fig. 1c. The maximum concentrations appear in mid-latitudes in the Northern Hemisphere where the source exists near the surface. The concentrations in the Southern Hemisphere are considerably lower. There is an approximately logarithmic decrease of concentration with height since the only sources are located at the earth's surface. The relatively large values centered around 15°S in the middle and upper troposphere coincide very well with the ascending region of the Hadley cell in the model (not shown). These features are common in all the three panels of Fig. 1 and agree well with results from many other models. The simulated values are within the range of inter-model variation in most regions (see, e.g., Jacob et al., 1997; Rasch et al., 2000).

There are also unrealistic aspects in the results, however. Both the TSPAS and MPDATA scheme produce evident high values of radon concentration near the North Pole in the middle and upper troposphere, showing a peak around 85°N. A similar phenomenon also appears in austral winter near the Antarctic, although the biases are not as pronounced (not shown). These high concentrations are unrealistic since there is neither emission from 70°N or 60°S poleward, nor sys-

tematic ascending motions in the polar regions. They are also inconsistent with the results from most other models.

This kind of error is not negligible although it appears only in relatively small regions compared to the global domain. High latitude areas in the middle and upper part of the troposphere are key regions for many chemical species. Ozone, for example, is both abundant and active in the polar regions and involved in a series of important chemical reactions taking place in the polar winter. The spurious high concentration noted above may possibly lead to large errors when various chemical species are included in the AGCM. Consequently they will result in an unrealistic simulation of the atmospheric components, not only because of the errors in transport, but also as a result of the biased chemical reactions.

It is worth noticing that in this test, the result obtained with the FFSL advection scheme (last panel of Fig. l) is free of the aforementioned biases in the polar regions. Given that large-scale advection is the only difference among the three realizations, it is reasonable to look for the causes of error via investigation of the properties of the advection schemes. A distinct feature of the FFSL scheme is that the semi-Lagrangian approach makes it much less restrictive in the stability constraint in the polar regions in comparison with the other two schemes. However, since the simulations are carried out with the Courant number less than unity even near the poles, the Courant criterion should not be the reason for the differences. It will be shown in the next section that inconsistency between the advection schemes and the discrete continuity equation in the dynamical core of the atmospheric model is possibly the reason that leads to the significant errors detected.

3. The consistency issue

To investigate the cause of the biases detected in section 2, we start from discussions on the generic transport problem in atmospheric models. If the distribution of a tracer is affected only by the transport process with no external sources or sinks, the mass of the tracer is conserved. This conservation law can be formulated in a generic pressure-based vertical coordinate η as

$$\frac{\partial}{\partial t}\left(q\frac{\partial p}{\partial \eta}\right)+\nabla\cdot\left(q\frac{\partial p}{\partial \eta}\boldsymbol{V}\right)=0\,. \tag{1}$$

Here q denotes the mixing ratio of the tracer, p the air pressure and $\boldsymbol{V}$ the 3-dimensional wind vector. By setting q to a constant value, we obtain

$$\frac{\partial}{\partial t}\left(\frac{\partial p}{\partial \eta}\right)+\nabla\cdot\left(\frac{\partial p}{\partial \eta}\boldsymbol{V}\right)=0\,. \tag{2}$$

This is nothing more than the continuity equation, which describes conservation of total mass of the atmosphere. $\partial p/\partial\eta$ is the pseudo density in a hydrostatic system which is proportional to air density in a height coordinate and equals the surface pressure in a sigma-coordinate. Combining Eqs. (1) and (2), we get

$$\frac{\partial q}{\partial t}+\boldsymbol{V}\cdot\nabla q=0\,, \tag{3}$$

which implies that a spatially uniform distribution of tracer will be preserved. Eqs. (1) and (3) are usually called the flux form and the advective form of the tracer conservation law, respectively.

In order to conserve tracer mass, usually the flux form Eq.(1) is discretized to construct a numerical scheme to predict q. The values of $(q\partial p/\partial\eta)$ and $\partial p/\partial\eta$ at the new time step are calculated using Eqs. (1) and (2) independently, then the quotient is taken to obtain the value of q. Let Q and π denote the discrete solutions of $(q\partial p/\partial\eta)$ and $\partial p/\partial\eta$, respectively. Suppose Eqs. (1) and (2) are discretized using the following formulas to solve q in an AGCM:

$$Q^{n+m}-Q^n=-m\Delta t F^n(\boldsymbol{V},Q)\,, \tag{4}$$

$$\pi^{n+m}-\pi^n=-m\Delta t G^n(\boldsymbol{V},\pi)\,, \tag{5}$$

where n and m are positive integers denoting the time step index, and Δt is the time step. (Please note that in this paper, superscripts in the formula always denote the time step index unless further notice.) If we assume the time integration scheme is explicit for the tracer, then F^n may involve values of the mixing ratio at the nth and earlier time steps, but no unknown values in the future. Furthermore we assume $F^n(\beta Q)=\beta F^n(Q)$ holds for an arbitrary positive constant β. (These two assumptions are true not only for all the three advection schemes in GAMIL, but also for many other advection schemes). In case q has a non-trivial constant value at all the previous time steps, we will have

$$\begin{aligned} q^{n+m}-q^n &\equiv \frac{Q^{n+m}}{\pi^{n+m}}-\frac{Q^n}{\pi^n}\\ &=\frac{m\Delta t}{\pi^{n+m}\pi^n}\left[Q^nG^n(\boldsymbol{V},\pi)-\pi^nF^n(\boldsymbol{V},Q)\right]\\ &=m\Delta t\mathcal{R}_c\frac{q^n}{\pi^{n+m}}\,. \end{aligned} \tag{6}$$

The consistency residual $\mathcal{R}_c$ in Eq.(6) is defined as

$$\mathcal{R}_c\equiv G^n(\boldsymbol{V},\pi)-F^n(\boldsymbol{V},\pi)\,. \tag{7}$$

Since $m\Delta t$ and q^n is never zero, the temporal increment of q will be zero if and only if $\mathcal{R}_c$ is zero. In other words, if the numerical approximation to Eq. (1) does not degenerate to the discrete continuity equation for $q = 1$, spurious sources and sinks will be generated in the discrete analogue of Eq. (3).

Traditionally, numerical schemes for advection processes are constructed with the assumption that the other variables in the transport equation are obtained by some independent external procedures. When these advection schemes are later adopted in an AGCM, the numerical methods used in the advection scheme and in the circulation model can be entirely different. Degeneration of the discrete tracer conservation to the continuity equation of air is therefore not guaranteed. As addressed in Jöckel et al. (2001), Rotman et al. (2004) and highlighted in Hourdin and Armengaud (1999), consequences of this inconsistency in long simulations could be severe if no special "fixing" is performed.

In the following, the consistency between the dynamical core of GAMIL and the advection schemes mentioned in section 1 is investigated. For simplicity and without loss of generality, all the formulas are written in one-dimensional form in the theoretical analysis.

Let u denote the wind velocity along the x axis and Δx be the grid size. For a generic variable ϕ, define the finite-difference operator $\delta_x(\cdot)$ and the averaging operator $\overline{(\cdot)}^x$ as

$$\delta_x(\phi_i) \equiv \frac{\phi_{i+\frac{1}{2}} - \phi_{i-\frac{1}{2}}}{\Delta x}$$

$$\overline{\phi}^x_{i+\frac{1}{2}} \equiv \frac{\phi_{i+1} + \phi_i}{2} ,$$

respectively. The subscript i is the spatial indice of the grid point along the x axis. With these notations and $m = 1$, the discrete continuity equation in GAMIL can be compactly written as

$$\pi_i^{n+1} - \pi_i^n = -\Delta t G_i^n(u, \pi) \equiv -\Delta t \mathcal{A}^n[\mathcal{S}_i(u, \pi)] . \quad (8)$$

In Eq. (8) we have decomposed G_i^n into a temporal operator $\mathcal{A}^n$ and a spatial operator $\mathcal{S}_i$

$$\mathcal{S}_i^n(u, \pi) \equiv \delta_x \left(u^n \overline{\pi^n}^x\right)_i , \quad (9)$$

while $\mathcal{A}^n$ stands for a two time level semi-implicit scheme (Wang and Ji, 2006) of which the details are given in Appendix A.

Similarly, the TSPAS scheme can be formulated as

$$Q_i^{n+1} - Q_i^n = -\Delta t F_T^n(u, Q) \equiv -\Delta t \tilde{\mathcal{A}}^n[\tilde{\mathcal{S}}_i(u, Q)] \quad (10)$$

with

$$\tilde{\mathcal{A}}^n(\tilde{\mathcal{S}}_i) \equiv \tilde{\mathcal{S}}_i^n , \quad (11)$$

$$\tilde{\mathcal{S}}_i^n(u, Q) \equiv \delta_x(u\overline{Q^n}^x)_i - \frac{1}{2}\delta_x(\mathscr{T}_i^n) , \quad (12)$$

and

$$\mathscr{T}^n_{i+\frac{1}{2}} \equiv |\tilde{u}|_{i+\frac{1}{2}}(Q^n_{i+1} - Q^n_i) . \quad (13)$$

Expression for the pseudo velocity $|\tilde{u}|^n_{i+\frac{1}{2}}$ can be found in Yu (1994). The MPDATA scheme consists of a series of consecutive iteration steps that can be written as

$$Q_i^{*^{k+1}} - Q_i^{*^k} = -\Delta t \hat{\mathcal{A}}^k[\hat{\mathcal{S}}_i(\hat{u}, Q^*)]$$

with

$$\hat{\mathcal{A}}^k(\hat{\mathcal{S}}_i) \equiv \hat{\mathcal{S}}_i^k \quad (15)$$

$$\hat{\mathcal{S}}_i^k(\hat{u}, Q^*) \equiv \delta_x\Big(\hat{u}^{k+1}\overline{Q^{*^k}}^x\Big)_i - \frac{1}{2}\delta_x(\mathscr{M}_i^k) , \quad (16)$$

and

$$\mathscr{M}^k_{i+\frac{1}{2}} \equiv \left|\hat{u}^{k+1}_{i+\frac{1}{2}}\right| (Q^{*^k}_{i+1} - Q^{*^k}_i) . \quad (17)$$

Here $k = 0, \ldots,$ IORD-1, where IORD indicates the number of corrective iterations Q^* such that

$$Q^{*^0} \equiv Q^n ; \quad Q^{*\mathrm{IORD}} \equiv Q^{n+1} .$$

IORD=3 is used in GAMIL. Expression for $\hat{u}^{k+1}_{i+\frac{1}{2}}$ can be found in Smolarkiewicz (1984), Smolarkiewicz and Clark (1986) and Smolarkiewicz and Grabowski (1990).

In our experiments the time step leads to Courant number less than unity at all gridpoints. The FFSL scheme with piecewise linear approximation, which is the algorithm used to produce results in Fig. 1c, can be summarized as

$$Q_i^{n+1} - Q_i^n = -\Delta t F_T^n(u, Q) \equiv -\Delta t \breve{\mathcal{A}}^n[\breve{\mathcal{S}}_i(u, Q)] \quad (18)$$

in which

$$\breve{\mathcal{A}}^n(\breve{\mathcal{S}}_i) \equiv \breve{\mathcal{S}}_i^n \quad (19)$$

$$\breve{\mathcal{S}}_i^n(u, Q) \equiv \delta_x(u, \overline{Q^n}^x)_i - \frac{1}{2}\delta_x(\mathscr{F}_i^n) + \frac{1}{2}\delta_x(\mathscr{H}_i^n) \quad (20)$$

Derivation of Eq. (20) and the detailed expression of $\mathscr{F}$ and $\mathscr{H}$ are given in Appendix B. For the subsequent discussion it is important to note that the last two terms on the right-hand-side of Eq. (20) will vanish if q is spatially constant.

With all these formulas above, we are able to compare the discretizations in the tracer advections schemes and the mass conservation equation in the general circulation model. To facilitate the analyses, we will consider the temporal and spatial operators separately.

Comparing Eqs. (9), (12), (16) and (20), it is not difficult to see that by setting $q^n = 1$:

- For the FFSL scheme with piecewise linear approximation, two terms in Eq. (20) vanishes and $\check{\mathcal{S}}_i^n(u, Q)$ equals $\mathcal{S}_i^n(u, \pi)$ When the piecewise parabolic method (PPM) is used in the FFSL scheme, it is not easy to summarize the formulation into a form like Eq. (20) for arbitrary distribution of q. However, it can still be proven that in case $q = 1$, we also have $\check{\mathcal{S}}_i^n(u, Q) = \mathcal{S}_i^n(u, \pi)$ no matter which monotonicity constraint is used.

- For TSPAS,

$$\tilde{\mathcal{S}}_i^n(u, Q) = \mathcal{S}_i^n(u, \pi) - \frac{1}{2}\delta_x(\mathscr{T}_i^n) \,, \tag{21}$$

  Since GAMIL uses the generalized sigma coordinate, $\pi = p_\mathrm{s} - p_\mathrm{T}$ where p_s and p_T are the pressure values at the earth's surface and the model top, respectively. The residual $R_\mathrm{T} = -\frac{1}{2}\delta_x(\mathscr{T}_i^n)$ is nontrivial wherever the wind velocity is not zero and horizontal gradient exists in the surface pressure field.

- For MPDATA, $\hat{\mathcal{S}}_i(\hat{u}, Q^*)$ (Eq. 16) does not degenerate to $\mathcal{S}_i(u, \pi)$ not only because of the residual $R_\mathrm{M} = -\frac{1}{2}\delta_x(\mathscr{M}_i^k)$, but also because of the difference between the real velocity u and the pseudo velocity $\hat{u}$ in the first term of Eq. (17).

Therefore in regard to the spatial operator, the FFSL scheme is consistent with the dynamical core of GAMIL while TSPAS and MPDATA are not. The inconsistency associated with MPDATA is more severe than TSPAS.

Now consider the temporal operator. First it should be pointed out that when TSPAS and FFSL are implemented in our model, the wind field at time step $n + \frac{1}{2}$ (defined as the arithmetic average of time step n and $n + 1$) is used in Eqs. (12) and (20) to achieve the second order accuracy. Comparing Eqs. (11), (15) and (19) with the time stepping scheme of the dynamical core and taking into account the iterative feature of MPDATA, we can conclude that none of the three advection schemes are advanced in time in the same manner as the continuity equation in GAMIL. This will cause errors to Eq. (3) regardless of which scheme is implemented in the model.

Table 1. Result of the constant tracer test using 3 different advection schemes (units: kg kg^{-1}).

Level	max or min	TSPAS	MPDATA	FFSL
Lowest layer	max	1.096	1.081	1.001
Lowest layer	min	0.828	0.737	0.997
Highest layer	max	1.364	1.689	1.001
Highest layer	min	0.719	0.577	0.997

In order to validate the analysis above, a constant tracer test is conducted. The GAMIL model with three different advection schemes is initialized with typical meteorological fields in January and a constant tracer mixing ratio of 1.0 kg kg^{-1} at all grid points. Since the true solution is exactly 1.0, the relative consistency error at each grid point can be defined as

$$\mathscr{E}_c = |q_i^n - 1.0| \,. \tag{22}$$

Figure 2 shows the relative consistency error of the scheme at the highest model level after 50 time steps (i.e., 200 minutes). Large errors appear in the polar regions, especially in the Northern Hemisphere for the TSPAS and MPDATA scheme. The maximum relative error on this level is more than 30% for TSPAS and nearly 70% for MPDATA, while the errors associated with FFSL is no larger than 0.3% (Table 1).

Figure 3 is the sigma-latitude cross section of the same quantity at 76°W, the longitude near which the Andes is located. The noise throughout all the model levels generated by TSPAS near 15°S is apparently associated with the steep and narrow mountain. Errors of the MPDATA scheme are larger than TSPAS in magnitude and affect more grid points especially in the middle and upper atmosphere.

Results of the idealized numerical experiment agree very well with our theoretical analysis. From Eqs. (13) and (17) we can expect that the residuals R_T and R_M will deviate significantly from zero when strong perturbations appear. Over the Andes, the dramatic change of surface pressure with topography is the main reason for large residuals. In the polar regions, the finite difference discretization without polar filtering produces circulations that are much less smooth than in, for example, spectral models. The differences between the zonal wind at neighboring grid points are of the same magnitude as in mid-latitudes. However, due to the convergence of the meridians, the zonal grid interval near the poles is about one tenth of that near the equator, resulting large values of the residuals. The FFSL scheme, on the other hand, has zero residual by design when $q = 1$ and, thus, differs from the continuity equation of the model only in temporal integration and

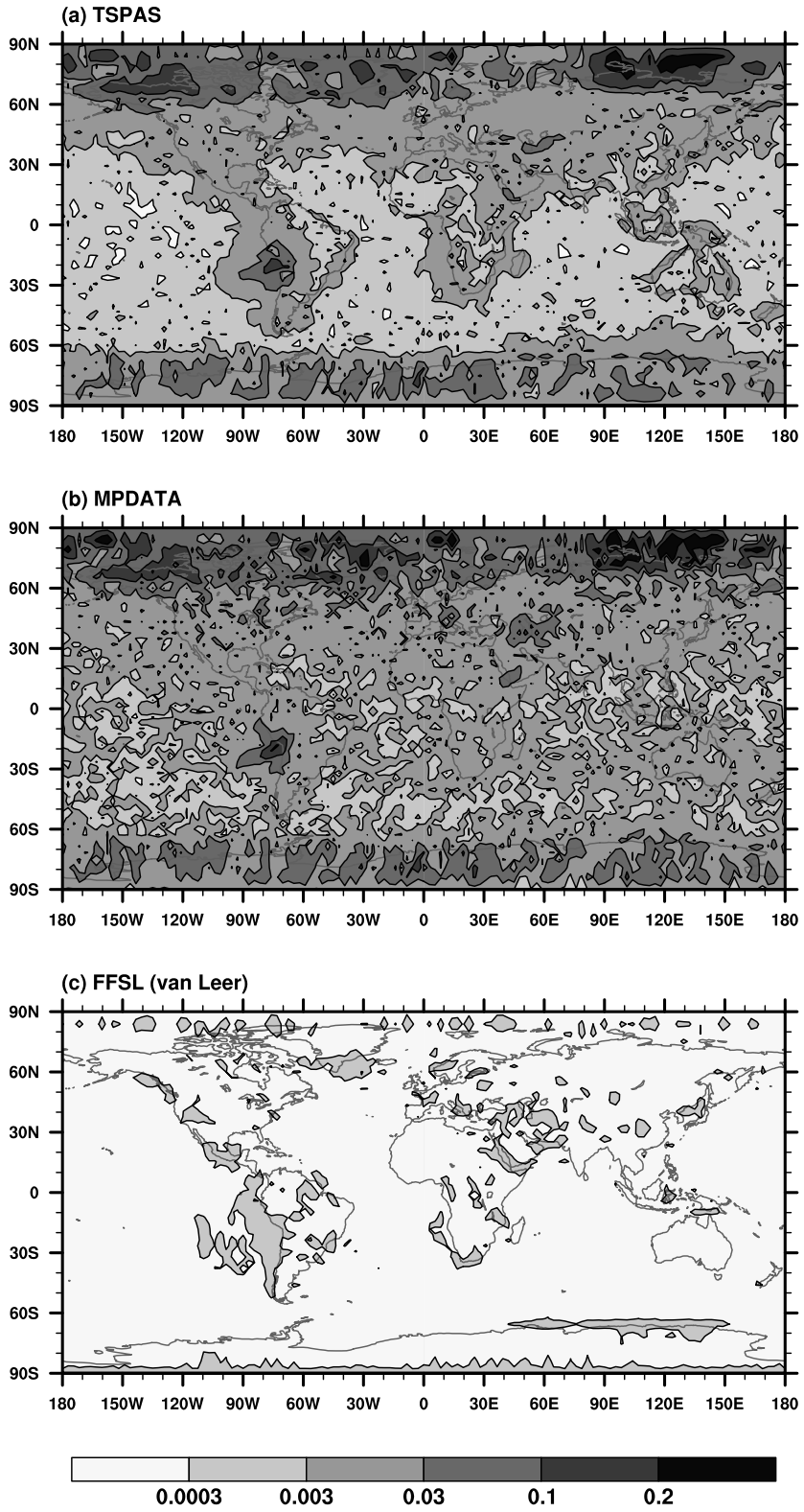

Fig. 2. Geograpical distribution of the absolute Relative Consistency Error (RCE) at the highest vertical level after 50 dynamical steps (200 minutes) in the constant tracer test with GAMIL using the (a) TSPAS, (b) MPDATA, and (c) FFSL (van Leer) advection scheme. (units: kg kg^{-1})

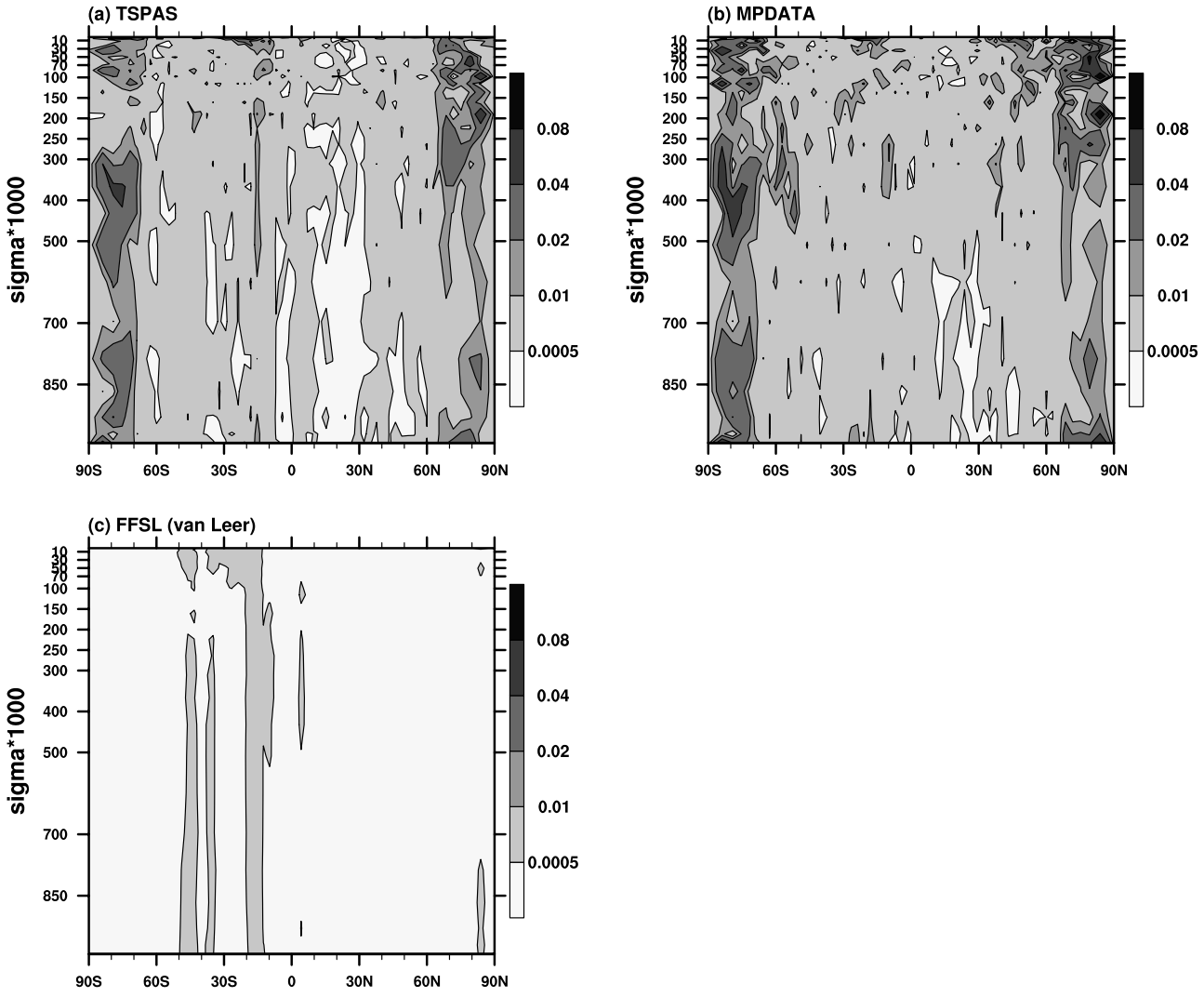

Fig. 3. Sigma-latitude cross section of the absolute Relative Consistency Error (RCE) at 76°W after 50 dynamical steps (200 minutes) in the constant tracer test with GAMIL using the (a) TSPAS (b) MPDATA and (c) FFSL (van Leer) advection scheme. (units: kg kg^{-1}). To get a natural comparison, model results are plotted on original sigma levels, but pressures of these sigma levels are also roughly indicated.

generates much smaller errors (Fig. 2c and Fig. 3c).

It should be noted that the consistency error shown here is in fact a quantitative estimate of the spurious source in the tracer transport equation. The spatial distributions of errors in the constant tracer test agree very well with the biases detected in the radon transport test, which confirms our attribution of those biases to the consistency issue.

4. Correlation between different species

In section 3 we have seen that if the consistency between the conservation of the tracer mass and that of the air mass is violated in an atmospheric model, significant errors may occur in the transport process of a single species. Moreover, it can be seen from Eq. (3) that in the continuous form, when two species are transported simultaneously, the initially linearly correlated concentrations will be retained in spite of the evolution with time. Since the early 1990s, tight correlations between tracers have been detected in high quality aircraft observations (Plumb and Ko, 1992). These correlations provide fundamental information about atmospheric transport and chemistry, which stresses the necessity of maintaining the linearity of an advection scheme for the tracer mixing ratio. Much attention has been paid to this issue in recent years (e.g., Lin and Rood, 1996). Assume the numerical schemes

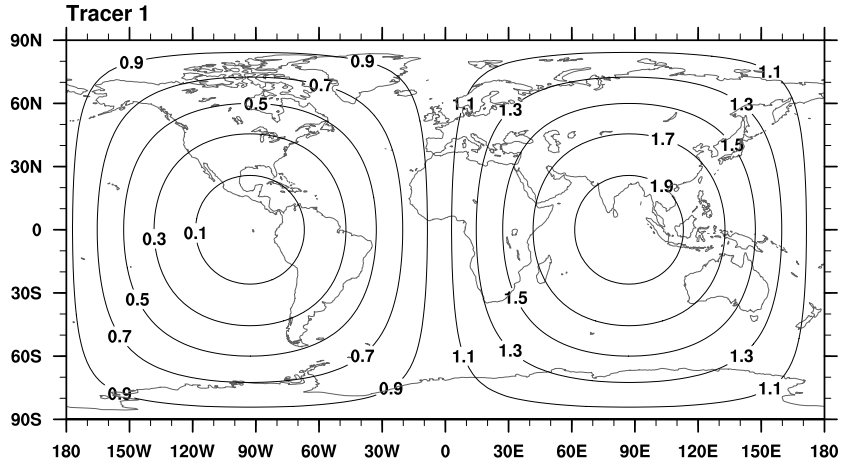

Fig. 4. The initial mixing ratio of tracer 1 in the tracer correlation test. (Units: kg kg^{-1})

Eqs. (4)–(5) are employed to simulate the transport of two species with mixing ratios q_1 and q_2 satisfying

$$q_1 = \gamma q_2 + \mu \tag{23}$$

at the nth time step where γ and μ are constants. By rewriting Eq. (4) as

$$q_1^{n+m}\pi^{n+m} = q_1^n\pi^n - m\Delta t F^n(\boldsymbol{V}, q\pi) \tag{24}$$

and using Eqs. (23) and (5), we obtain

$$\begin{aligned} q_1^{n+m}\pi^{n+m} =& (\gamma q_2^{n+m} + \mu)\pi^{n+m} \\ &+ \mu m\Delta t\mathcal{R}_{\rm c} + m\Delta t\mathcal{R}_{\rm s}\,. \end{aligned} \tag{25}$$

Here $\mathcal{R}_{\rm c}$ is the consistency residual given by Eq. (7). The split residual $\mathcal{R}_{\rm s}$ is defined as

$$\begin{aligned} \mathcal{R}_s =& F^n(\boldsymbol{V}, \gamma q\pi) + F^n(\boldsymbol{V}, \mu\pi) - \\ & F^n[\boldsymbol{V}, (\gamma q + \mu)\pi]\,. \end{aligned} \tag{26}$$

Given that μ is not necessarily zero, $\mathcal{R}_{\rm c} = 0$ and $\mathcal{R}_{\rm s} = 0$ are the necessary conditions to retain (23) at the new time step. The former has already been discussed in detail in the previous section, while the latter may be violated when additional mononicity constraints are imposed on the advecion scheme.

We now perform another idealized test, again using the GAMIL model with three different advection schemes. Two tracers are transported simultaneously in this experiment with initial conditions given by

$$q_1^0 = 1 + \sin\lambda\cos\varphi\,,\ \ q_2^0 = 1 - \sin\lambda\cos\varphi\,,$$

respectively (Fig. 4), where λ is the longitude and φ the latitude. We define the tracer correlation error

$$\mathscr{E}_r = \frac{1}{2}|q_1^n + q_2^n - 2.0| \tag{27}$$

to evaluate the extent to which the relationship between the two species is violated. The correlation error associated with TSPAS and MPDATA scheme at the highest model level after 50 time steps (200 minutes) is shown in Figs. 5a, b. The error given by FFSL is much smaller (Fig. 5c). Spatial features of the correlation error are quite similar to the consistency error in Fig. 2 because the consistency residual is considerably larger than the split residual in these two schemes, which again highlights the necessity to reduce the consistency error in an atmospheric model.

5. Concluding remarks

In this study, the radon transport test is carried out using the atmospheric general circulation GAMIL with three different tracer advection schemes. Significant biases are detected with the TSPAS and MPDATA scheme in the polar regions and in the upper atmosphere. Theoretical investigation into the formulations of the schemes reveals that the inconsistency between the tracer advection scheme and the discrete continuity equation in the atmospheric model can lead to spurious sources and sinks of considerable magnitude to the tracer advection equation. This is identified via idealized numerical experiments as the cause of the biases in the radon test. Additional analysis and experiments show that this inconsistency can also lead to severe violation of the linear relationship between different species. When the mixing ratio is spatially uniform with value 1.0, the FFSL advection scheme degenerates to the same form as the discrete continuity equation in the GAMIL model in terms of spatial discretization, thus dramatically reduces the inconsistency and the consequent errors.

These results are quite informative and give us useful hints for choosing appropriate advection schemes

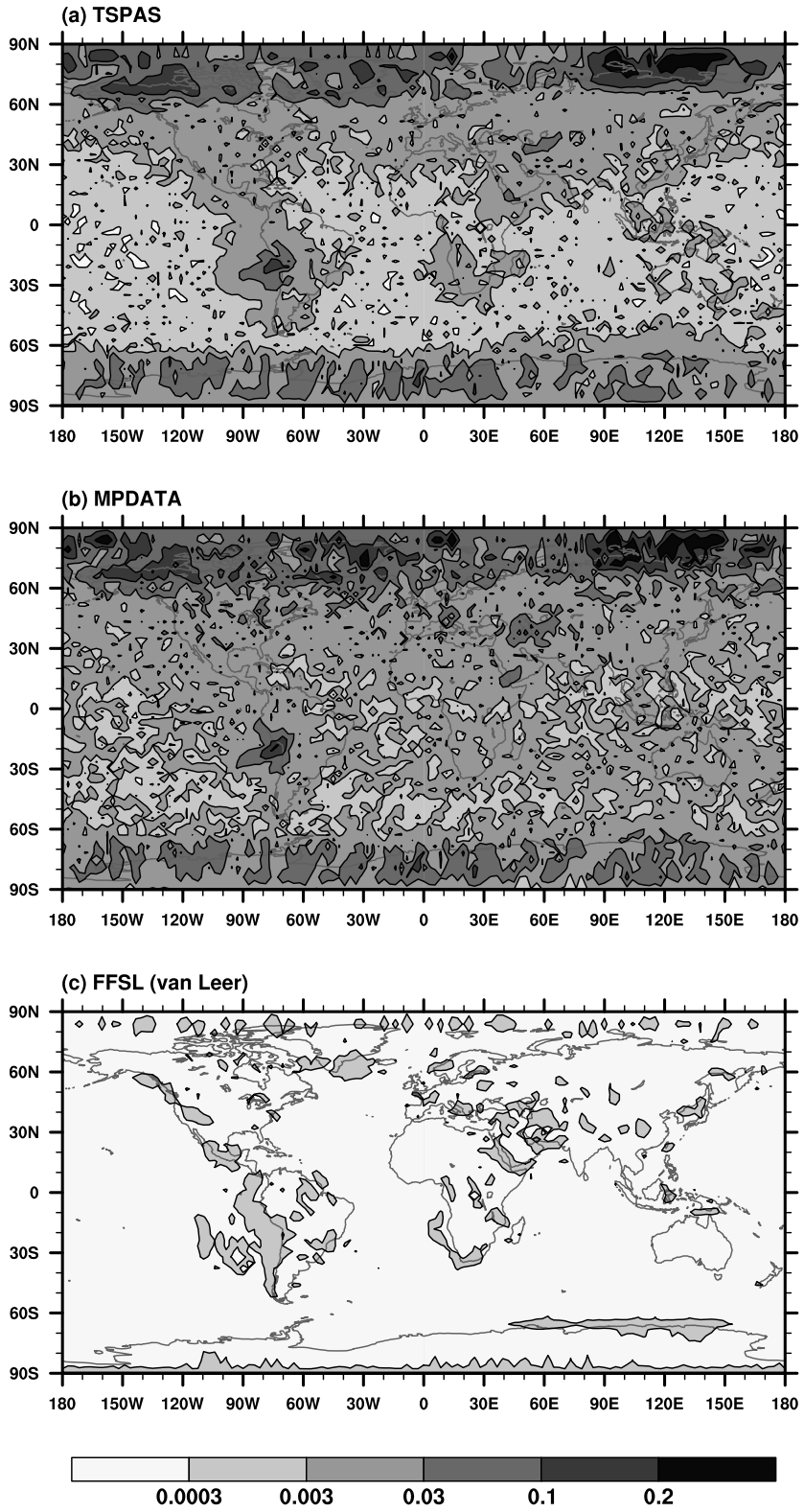

Fig. 5. Geograpical distribution of the absolute Tracer Correlation Error (TCE) at the highest vertical level after 50 dynamical steps (200 minutes) in the tracer corelation test with GAMIL using the (a) TSPAS (b) MPDATA and (c) FFSL (van Leer) advection scheme. (units: kg kg^{-1})

in the GAMIL model. Although both the TSPAS and MPDATA have been adopted in GAMIL and demonstrated reasonable performance for water vapor transport with regard to the feedback on the general circulation, they had not been evaluated for other species before this study. Recently a module describing the aerosol-related physical and chemical processes has be designed for GAMIL. Implementation of this new module inevitably involves introduction of many new species that either are chemically active or have significant impact on the physical system. Results from this work implies that at least for those closely correlated species as well as those having high concentrations in the polar regions, the FFSL scheme is more suitable for simulating the large-scale transport processes.

For water vapor, however, the performance of FFSL in the GAMIL model has not yet been evaluated in detail. There are some preliminary results showing that use of FFSL helps to improve the simulated temperature field and cloud fraction in the polar regions. Since water vapor is one of the essential components of the atmosphere, a comprehensive evaluation and comparison of the currently available advection schemes is planned with focus on the hydrologic cycle.

Currently the FFSL package is implemented in the AGCM in such a way that the total mass of the tracer will be conserved to machine precision if there is no external source or sink. The constant tracer test reveals that the magnitude of the relative consistency error [defined by expression (22) associated with the FFSL scheme in GAMIL is about] 0.3%. This is introduced by the different time integration algorithms in FFSL and in the dynamical core. To entirely remove this error, the pseudo density of the air, which is needed for converting tracer pseudo density to the mixing ratio, can be recalculated using the same time integration scheme as in FFSL. However, the difference between the recalculated density and the value computed in the dynamical core will result in a slight violation of the total mass conservation of the tracer. The exactly conservation of tracer mass and elimination of spurious sources of the mixing ratio is hence a dilemma. An ultimate solution of this problem would be to use exactly the same time marching method for the dynamical core and for the advection scheme. This can be done, for example, by applying the time integration algorithm Eqs. (28)–(30) in Appendix A to Eqs. (31) in Appendix B. However, as a consequence, there is an additional computational expense due to the iterative feature of Eqs. (28)–(30). If a number of species are to be transported in this way, the CPU time needed will increase quite considerably and may even render the scheme unaffordable. It does not seem worth the greater expense to reduce a very small error, especially for species that have strong external sources and sinks. Complete consistency can be achieved, on the other hand, by applying the flux-form semi-Lagrangian idea to the continuity equation, although one needs to be very careful to preserve the total energy conservation which is an important feature of the GAMIL dynamical core. Further studies are planned to address this issue.

Acknowledgements. The authors are grateful to both of the two anonymous reviewers for their constructive comments and suggestions. We acknowledge the financial support from the 973 project with Grant No. 2005CB321703, the Fund for Innovative Research Groups with Grant No. 40221503 and the CAS International Partnership Creative Group "The Climate, System Model Development and Application Studies".

APPENDIX A

Time Integration Scheme for the Continuity Equation in GAMIL

For simplicity, we write the spatially discretized continuity equation of the GAMIL model in 2D form as

$$\frac{\partial \pi}{\partial t} = -\delta_x(u\overline{\pi}^x)_i - \delta_y(v\overline{\pi}^y)_j$$

where π denotes the pseudo density in the sigma coordinate. Three sub-steps are performed to update the value of π from time level n to level $n+1$:

$$\pi_{(1)}^{n+\frac{1}{2}} = \pi^n - \frac{\Delta t}{2}\delta_x\left[\tilde{u}^{n+\frac{1}{2}}\overline{(\tilde{\pi}^{n+\frac{1}{2}})}^x\right]_i - \frac{\Delta t}{2}\delta_y\left[v^n\overline{(\pi^n)}^y\right]_j , \tag{A1}$$

$$\pi_{(2)}^{n+\frac{1}{2}} = \pi^n - \frac{\Delta t}{2}\delta_x\left[\tilde{u}_{(1)}^{n+\frac{1}{2}}\overline{\left(\tilde{\pi}_{(1)}^{n+\frac{1}{2}}\right)}^x\right]_i - \frac{\Delta t}{2}\delta_y\left[v_{(1)}^{n+\frac{1}{2}}\overline{\left(\pi_{(1)}^{n+\frac{1}{2}}\right)}^y\right]_j , \tag{A2}$$

$$\pi^{n+1} = \pi^n - \Delta t\beta^n\delta_x\left[\tilde{u}_{(1)}^{n+\frac{1}{2}}\overline{\left(\tilde{\pi}_{(1)}^{n+\frac{1}{2}}\right)}^x\right]_i - \Delta t\beta^n\delta_y\left[v_{(2)}^{n+\frac{1}{2}}\overline{\left(\pi_{(2)}^{n+\frac{1}{2}}\right)}^y\right]_j . \tag{A3}$$

Here the subscripts (1) and (2) denote the first guess and the correction, respectively. Variables with a tilde

are the estimates obtained by implicitly solving the 1D external gravity wave equation in the zonal direction. β^n is a time-dependent parameter which has not spacial variation. A complete description of the time stepping scheme as well as the basic idea of it can be found in Chapter 9 of Wang and Ji (2006) and in Wang et al. (2004).

APPENDIX B

FFSL Scheme with Piecewise Linear Approximation

The FFSL scheme with piecewise linear approximation (i.e., the van Leer type algorithm) has been detailed in LR96. For simplicity, the formulation was given for nondivergent flow and $\pi =$ constant in which the tracer density Q and mixing ratio q were interchangable. However, for practical use in the AGCMs, especially for the consistency issue being discussed in this paper, it is essential to distinguish Q and q clearly and modify the related operators properly. Therefore we rewrite here the formulas in LR96 and manipulate them further into the form presented in section 3.

The 2D FFSL scheme in the C-grid system can be written in symbolic form as

$$\frac{Q^{n+1}-Q^n}{\Delta t} = -\delta_x\left\{\mathscr{X}\left[q^n+\frac{1}{2}g(q^n)\right]\right\} - \delta_y\left\{\mathscr{Y}\left[q^n+\frac{1}{2}f(q^n)\right]\right\}. \quad \text{(B1)}$$

The finite difference operator $\delta_x(\cdot)$ is the same as in section 3 and $\delta_y(\cdot)$ is defined similarly for the other direction. $\mathscr{X}$ and $\mathscr{Y}$ are the mass fluxes of the tracer in the east-west and north-south direction, respectively, but has modified expression comparing to LR96. Following that paper, we focus only on the first term on the right-hand-side of (B1).

The advective-form operator $g(q^n)$ is defined at gridpoint (i,j) as

$$g_{i,j} = (q^n_{i,J} - q^n_{i,j}) + |c^y_{i,j}|(q^n_{i,J^*} - q^n_{i,J}),$$

where

$$C^y_{i,j} = \frac{\Delta t}{2\Delta y}\left(v_{i,j-\frac{1}{2}} + v_{i,j+\frac{1}{2}}\right),$$

$$c^y_{i,j} = C^y_{i,j} - \mathrm{int}(C^y_{i,j}),$$

$$J = j - \mathrm{int}(C^y_{i,j}),$$

$$J^* = J - \mathrm{sign}(1, C^y_{i,j}).$$

Here $C^y_{i,j}$ and $c^y_{i,j}$ are the Courant number in the y-axis direction and its fractional part, respectively.

Define an intermediate quantity

$$q^*_{ij} = q^n_{i,j} + \frac{1}{2}g_{i,j}(q^n).$$

When the Courant number is less than unity, the "integer part" of flux $\mathscr{X}$ defined in LR96 vanishes, and the fractional part computed by the van Leer scheme is

$$\mathscr{X}_{i+\frac{1}{2},j} = u_{i+\frac{1}{2},j}\overline{(\pi^n)}^x_{i+\frac{1}{2},j}\left\{q^*_{I,j} + \frac{\Delta q^*_{I,j}}{2}\left[\mathrm{sign}\left(1, c^x_{i+\frac{1}{2},j}\right) - c^x_{i+\frac{1}{2},j}\right]\right\}, \quad \text{(B2)}$$

where

$$c^x_{i+\frac{1}{2},j} = \frac{\Delta t}{\Delta x}u_{i+\frac{1}{2},j}$$

and

$$I = i + 1 - \mathrm{int}\left(c^x_{i+\frac{1}{2},j}\right).$$

$\Delta q^*_{I,j}$ can be calculated simply by

$$\Delta q^*_{I,j} = \frac{1}{2}\left(q^*_{I+1,j} - q^*_{I-1,j}\right)$$

or with a monotinicity constraint as in Lin et al. (1994).

So far we have rewritten the van Leer type formulation in LR96 for divergent flow. In the following, we further manipulate (B2) to reveal the relation between this scheme with the dynamical core of GAMIL. In the following formulas we omit the north-south direction index which is always j. Using the equality

$$u_{i+\frac{1}{2}}\overline{(\pi^n)}^x_{i+\frac{1}{2}}q^n_I = u_{i+\frac{1}{2}}\overline{(Q^n)}^x_{i+\frac{1}{2}} - |u|_{i+\frac{1}{2}}\pi^n_{I^*}\left(q^n_i - q^n_{i-1}\right),$$

we can obtain

$$-\delta_x\left\{\mathscr{X}\left[q^n+\frac{1}{2}g(q^n)\right]\right\} = \delta_x\left(u^n\overline{Q^n}^x\right)_i - \frac{1}{2}\delta_x(\mathscr{F}^n_i) + \frac{1}{2}\delta_x(\mathscr{H}^n_i)$$

where

$$\mathscr{F}^n_{i+\frac{1}{2}} = |u|_{i+\frac{1}{2}}\pi^n_{I^*}\left(q^n_{i+1} - q^n_i\right),$$

$$\mathscr{H}^n_{i+\frac{1}{2}} = u_{i+\frac{1}{2}}\pi^n_{i+\frac{1}{2}}\left\{g_I(q^n) + \Delta q^*_I\left[\mathrm{sign}(1, c^x_{i+\frac{1}{2}}) - c^x_{i+\frac{1}{2}}\right]\right\}.$$

The subscript I^* is defined as

$$I^* = \text{int}\left(i + 1 + \frac{\Delta t}{\Delta x} u_{i+\frac{1}{2}}\right) ;$$

the pseudo-density π in the sigma coordinate used by GAMIL is given by

$$\pi = p_{\text{s}} - p_{\text{T}} ,$$

where p_{s} and p_{T} denote the pressure values at the earth's surface and the model top, respectively. $\mathscr{F}$ is the counterpart of Eqs. (13) and (17), but with the crucial difference that the variable which appears in the brackets is now the mixing ratio instead of pseudo density of the tracer. When q is a constant, both $\mathscr{F}$ and $\mathscr{H}$ will become zero.

REFERENCES

Chin, M., R. B. Rood, S. J. Lin, J. F. Müller, and A. M. Thompson, 2000: Atmospheric sulfur cycle simulation in the global model GOCART: Model description and global properies. *J. Geophys. Res.*, **105**, 24617–24687.

Genthon, C., and A. Armengaud, 1995: Radon 222 as a comparative tracer of transport and mixing in two general circulation models of the atmosphere. *J. Geophys. Res.*, **100**(D2), 2849–2866.

Hourdin, F., and A. Armengaud, 1999: The use of finite-volume methods for atmospheric advection of trace species. Part I: Test of various formulations in a general circulation model. *Mon. Wea. Rev.*, **127**, 822–837.

Jacob, D. J., and M. J. Prather, 1990: Radon-222 as a test of convective transport in a general circulation model. *Tellus*, **42B**, 118–134.

Jacob, D. J., and Coauthors, 1997: Evaluation and intercomparison of global atmospheric transport models using ^{222}Rn and other short-lived tracers. *J. Geophys. Res.*, **102**(D5), 5953–5970.

Lin, S. J., and R. B. Rood, 1996: Multidimensional flux-form semi-Lagrangian transport schemes. *Mon. Wea. Rev.*, **124**, 2046–2070.

Lin, S.-J., W. C. Chao, Y. C. Sud, and G. K. Walker, 1994: A class of the van Leer-type transport schemes and its application to the moisture transport in a general circulation model. *Mon. Wea. Rev.*, **122**, 1575–1593.

Jöckel, P., R. Kuhlmann, M. G. Lawrence, B. Steil, C. A. M. Brenninkmeijer, P. J. Crutzen, P. J. Rasch, and B. Eaton., 2001: On a fundamental problem in implementing flux-form advection schemes for tracer transport in 3-dimensional general circulation and chemistry transport models. *Quart. J. Roy. Meteor. Soc.*, **127**(573), 1035–1052.

Plumb, R. A., and M. K. W. Ko, 1992: Interrelationships between mixing ratios of long-lived stratospheric constituents. *J. Geophys. Res.*, **97**, 10145–10156.

Rasch, P. J., and Coauthors, 2000: A comparison of scavenging and deposition processes in global models: Results from the WCRP Cambridge Workshop of 1995. *Tellus*, **52B**, 1025–1056.

Roeckner, E., and Coauthors, 2003: The atmospheric general circulation model ECHAM 5. PART I: Model description. MPI Technical Report 349, Max Planck Institute for Meteorology, Hamburg, Germany, 27–29.

Rotman, D. A., and Coauthors, 2001: Global modeling initiative assessment model: model description, integration and testing of the transport shell. *J. Geophys. Res.*, **106**(D2), 1669–1691.

Rotman, D. A., and Coauthors, 2004: Impact, the llnl 3-d global atmospheric chemical transport model for the combined troposphere and stratosphere: Model description and analysis of ozone and other trace gases. *J. Geophys. Res.*, **109**, D04303, doi:10.1029/2002JD003155.

Smolarkiewicz, P. K., 1984: A fully multidimensional positive definite advection transport algorithm with small implicit diffusion. *Journal Computational Physics*, **54**, 325–362.

Smolarkiewicz, P. K., and T. L. Clark, 1986: The multidimensional positive definite advection transport algorithm: further development and applications. *Journal Computational Physics*, **67**, 396–438.

Smolarkiewicz, P. K., and W. W. Grabowski, 1990: The multidimensional positive definite advection transport algorithm: Nonoscillatory option. *Journal Computational Physics*, **86**, 355–375.

Smolarkiewicz, P. K., and G. A. Grell, 1992: A class of monotone interpolation schemes. *J Comput. Phys.*, **101**, 431–440.

Wan, H., B. Wang, Y. Q. Yu, and R. C. Yu, 2006: Development and validation of the gridpoint atmospheric model of IAP LASG (GAMIL). Technical Report 16, LASG, Institute of Atmospheric Physics, Chinese Academy of Sciences, Beijing, P. R. China, 78pp.

Wang, B., and Z. Z. Ji, 2006: *New Numerical Methods in Atmospheric Sciences and Their Applications.* Science Press, Beijing, P. R. China, 208pp. (in Chinese)

Wang, B., H. Wan, Z. Z. Ji, X. Zhang, R. C. Yu, Y. Q. Yu, and H. T. Liu, 2004: Design of a new dynamical core for global atmospheric models based on some efficient numerical methods. *Science in China*(A), **47**(Suppl.), 4–21.

Yu, R. C., 1994: A two-step shape-preserving advection scheme. *Adv. Atmos. Sci.*, **11**(4), 479–490.

Uppala, S. M., and Coauthors, 2005: The ERA-40 reanalysis. *Quart. J. Roy. Meteor. Soc.*, **131**(612), 2961–3012.